XAS Structural Comparisons of Reversibly Interconvertible Oxo- and Hydroxo-Bridged Heme-Copper Oxidase Model Compounds

Stephen Fox,[†] Alaganandan Nanthakumar,[†] Mårten Wikström,[‡] Kenneth D. Karlin,*[,†] and Ninian J. Blackburn*[,§]

Contribution from the Department of Chemistry, The Johns Hopkins University, Charles and 34th Streets, Baltimore, Maryland 21218, Department of Medical Chemistry, FIN-00014, University of Helsinki, Finland, and Department of Chemistry and Biological Sciences, Oregon Graduate Institute, Beaverton, Oregon 97006

Received May 24, 1995[⊗]

Abstract: In this study on model compounds for the iron−copper dinuclear center in heme-copper oxidases, we (i) detail the synthesis and *reversible* acid−base interconversion of μ-oxo and μ-hydroxo complexes [(F_8-TPP)Fe^{III}−(O^{2-})−Cu^{II}(TMPA)]$^+$ (**1**) and [(F_8-TPP)Fe^{III}−(OH^-)−Cu^{II}(TMPA)]$^{2+}$ (**2**) [F_8-TPP = tetrakis(2,6-difluorophenyl)-porphyrinate(2−), TMPA = tris[(2-pyridylmethyl)amine]; (ii) compare their physical properties; (iii) establish the structure of **2** using XAS (X-ray absorption spectroscopy), a novel application of a three-body two-edge multiple-scattering (MS) analysis of ligand connectivity; and (iv) compare the XAS of **2** with those of **1** and an enzyme preparation. Complex **1** was prepared by reaction of [(TMPA)Cu^{II}(CH_3CN)]$^{2+}$ (**3**) and [(F_8-TPP)Fe^{III}−OH] (**4**) with triethylamine in acetonitrile (>70% yield). Salts **2**-(ClO_4)$_2$ and **2**-(CF_3SO_3)$_2$ were synthesized (>60% yield) by addition of **3** with **4** in dichloroethane or by protonation of **1** with triflic acid. In a ^{1}H-NMR spectroscopic titration (298 K) with triflic acid, the pyrrole 65 ppm resonance for **1** progressively converts to one near 70 ppm (71.5 for triflate, 68.5 for perchlorate), diagnostic of **2**. The protonation−deprotonation rate is slow on the NMR time scale, the ^{1}H-NMR spectral properties are consistent with antiferromagnetically coupled high-spin iron(III) and Cu(II) ions ($S = 2$ ground state), and the interaction is weaker in **2** (**2**, 5.5 ± 0.1 μ_B; **1**, 5.1 ± 0.1 μ_B, Evans method). UV−vis spectroscopy was also used to monitor the conversion of **2** (Soret, 410 nm) to **1** (434 nm) using Et_3N. The aqueous pK_a for deprotonation of **2** is estimated as 8 ± 2.5. Both Fe and Cu K-edge XAS was performed on **1**, **2**, and μ-peroxo complex [{(TMPA)Cu}$_2$(O_2)]$^{2+}$ (**5**). The strong MS interaction observed in the EXAFS of **1** is due to the nearly linear Fe−O−Cu moiety. Least-squares refinement of the Cu K-EXAFS of **1** gives Cu···Fe = 3.56 ± 0.03 Å, ∠Cu−O−Fe = 176 ± 5°, Cu−O = 1.83 ± 0.02 Å; the Fe K-EXAFS analysis gives Fe−O = 1.72 ± 0.02 Å, Fe···Cu = 3.54 ± 0.05 Å, ∠Fe−O−Cu = 172 ± 10°. The intense Fe−Cu (or Cu−Fe) feature is lacking in **2**, but the iron-edge spectra do reveal a weaker MS ascribed to the Fe−Cu interaction. The Cu−O(H) and Fe−O(H) bonds are elongated in **2** (1.89 ± 0.02 Å and 1.87 ± 0.02 Å, respectively), with Fe···Cu = 3.66 ± 0.03 Å. This protonated complex is bent; ∠Fe−O(H)−Cu = 157 ± 5°. An EXAFS comparison with an enzyme preparation of the quinol oxidase aa_3-600 from *Bacillus subtilis* supports the notion that μ-OH^- complex **2** may be a good heme-Cu enzyme model for the resting state and/or turnover intermediate.

Introduction

Among Nature's most intriguing enzyme functions having active-site chemistry involving metal-containing arrays is that found in heme-copper oxidases, which are ubiquitous respiratory proteins occurring in both prokaryotic and eukaryotic aerobic organisms.[1] They function to catalyze the four-proton four-electron reduction of dioxygen to water, and transduce the energy ($E° = +0.815$ V, pH 7, 1 atm of O_2) made available by coupling this O−O reductive cleavage reaction to the translocation of protons across the cytoplasmic or mitochondrial membrane (Figure 1).[2] Subsequent ATP synthesis harnesses the pH gradient and membrane potential energy.

The subunit I unique bimetallic heme-copper active center is (i) the site of O_2 binding and reduction and (ii) the site of redox-linked proton translocation, Figure 1. Biochemical and spectroscopic studies implicate three histidine imidazoles[5] and possibly a tyrosine[6] residue as Cu_B ligands; the histidine coordination has been confirmed by recent 2.8 Å resolution X-ray crystal structures.[7−9] The functional enzyme includes a fully reduced state; kinetic-spectroscopic investigations reveal that reaction with O_2 leads to Cu−O_2 and then Fe−O_2 initial

[†] Johns Hopkins University.
[‡] University of Helsinki, Finland.
[§] Oregon Graduate Institute.
[⊗] Abstract published in *Advance ACS Abstracts,* December 15, 1995.

(1) (a) García-Horsman, J. A.; Barquera, B.; Rumbley, J.; Ma, J.; Gennis, R. B. *J. Bacteriol.* **1994**, *176*, 5587−5600. (b) Calhoun, M. W.; Thomas, J. W.; Gennis, R. B. *Trends Biochem. Sci.* **1994**, *19*, 325−330. (c) van der Oost, J.; de Boer, A. P. N.; de Gier, J.-W. L.; Zumft, W. G.; Stouthamer, A. H.; van Spanning, R. J. M. *FEMS Microbiol. Lett.* **1994**, *121*, 1−10.

(2) (a) Morgan, J. E.; Verkhovsky, M. I.; Wikström, M. *J. Bioenerg. Biomembr.* **1994**, *26*, 599−608. (b) Babcock, G. T.; Wikström, M. *Nature* **1992**, *356*, 301−309. (c) Malmström, B. G. *Acc. Chem. Res.* **1993**, *26*, 332−338. (d) Larsen, R. W.; Pan, L.-P.; Musser, S. M.; Li, Z.; Chan, S. I. *Proc. Natl. Acad. Sci. U.S.A.* **1992**, *89*, 723−727. (e) Williams, R. J. P. *Nature* **1995**, *376*, 643.

(3) Recently discovered cytochrome cbb_3- or *cb*-type oxidases accept electrons from cytochrome *c*, but lack the Cu_A center. García-Horsman, J. A.; Berry, E.; Shapleigh, J. P.; Alben, J. O.; Gennis, R. B. *Biochemistry* **1994**, *33*, 3113−3119. Gray, K. A.; Grooms, M.; Myllykallio, H.; Moomaw, C.; Slaughter, C.; Daldal, F. *Biochemistry* **1994**, *33*, 3120−3127.

(4) (a) Antholine, W. E.; Kastrau, D. H. W.; Steffens, G. C. M.; Buse, G.; Zumft, W. G.; Kroneck, P. M. H. *Eur. J. Biochem.* **1992**, *209*, 875−881. (b) Kelly, M.; Lappalainen, P.; Talbo, G.; Haltia, T.; van der Oost, J.; Saraste, M. *J. Biol. Chem.* **1993**, *268*, 16781−16787. (c) Andrew, C. R.; Han, J.; de Vries, S.; van der Oost, J.; Averill, B. A.; Loehr, T. M.; Sanders-Loehr, J. *J. Am. Chem. Soc.* **1994**, *116*, 10805−10806. (d) Blackburn, N. J.; Barr, M. E.; Woodruff, W. H.; van der Oost, J.; de Vries, S. *Biochemistry* **1994**, *33*, 10401−10407.

0002-7863/96/1518-0024$12.00/0 © 1996 American Chemical Society

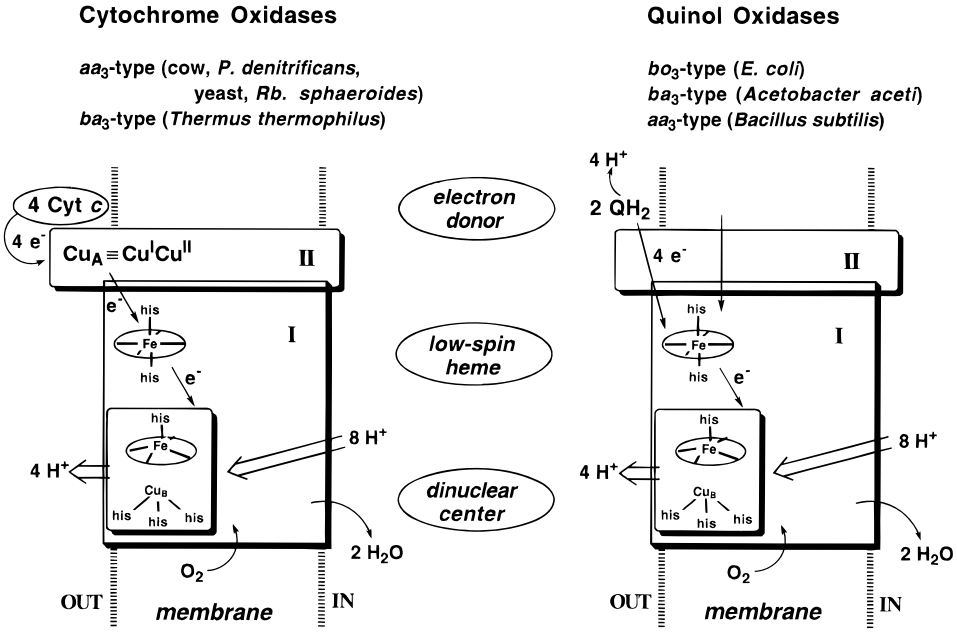

Figure 1. Catalytic "machinery" for the two major classes of the heme-copper oxidase superfamily.[3] The Cu_A center in cytochrome oxidases consists of a dinuclear mixed-valent center with cysteinate coordination.[4]

adducts, followed by (hydro)peroxo metal and ferryl (Fe═O) intermediates.[10] The protonation events during this sequence are clearly critical to the enzyme function; these active-site processes lead to the water product and a fully oxidized state, which may be equivalent to the resting-state and/or "as-isolated" enzyme form. This oxidized heme-copper center is suggested to consist of an EPR silent, (weakly or strongly) antiferromagnetically coupled $Fe^{III}-X-Cu_B^{II}$ moiety,[11] where X has variously been suggested to be an oxo (O^{2-}), hydroxo, chloro, sulfido, cysteinato, or imidazolato group. The resting form has been the subject of extensive investigations, including characterization of its physical properties (*vide supra*) and reactivity with anion sources or hydrogen peroxide.[12] Despite the recent crystallographic results,[7,8] it remains to be determined if magnetic/spectroscopic properties of isolated enzyme preparations correspond to the observed protein structures, i.e., with respect to the nature of the bridging ligand, if any, the heme $a_3\cdots Cu_B$ distance, and the precise coordination at Cu_B.[9,13]

The enigmatic nature of the heme-copper moiety has provoked considerable efforts by coordination chemists to generate synthetically derived models.[14] While some efforts have been directed toward O_2 reactivity with PFe^{II} (P = porphyrinate) and Cu^I complexes,[14a,15] most biomimetic modeling has concentrated upon oxidized $PFe^{III}-Cu^{II}L$ (L = copper ligand) heterodinuclear complexes.[14a−c] Synthetic approaches include the employment of porphyrins modified with covalently linked chelates for copper,[14a,15a,e,16] and $PFe^{III}-X-Cu^{II}L$ complexes made through various self-assembly strategies. Recent efforts in the latter direction include compounds with X = O^{2-}, OH^-, CN^-, and F^- ions.[14a,b,15c,17] $PFe^{III-}(CN^-)-$

(5) (a) Hosler, J. P.; Ferguson-Miller, S.; Calhoun, M. W.; Thomas, J. W.; Hill, J.; Lemieux, L.; Ma, J.; Georgiou, C.; Fetter, J.; Shapleigh, J.; Tecklenburg, M. J.; Babcock, G. T.; Gennis, R. B. *J. Bioenerg. Biomembr.* **1993**, *25*, 121−136. (b) Shapleigh, J. P.; Hosler, J. P.; Tecklenburg, M. M. J.; Kim, Y.; Babcock, G. T.; Gennis, R. B.; Ferguson-Miller, S. *Proc. Natl. Acad. Sci. U.S.A.* **1992**, *89*, 4786−4790. (c) Minagawa, J.; Mogi, T.; Gennis, R. B.; Anraku, Y. *J. Biol. Chem.* **1992**, *267*, 2094−2104. (d) Fang, Y. C.; Ahmad, I.; Blackburn, N. J.; Boswell, J. S.; Verkhovskaya, M. L.; Hoffman, B. M.; Wikström, M. *Biochemistry* **1995**, *34*, 10245−10255.

(6) (a) Thomas, J. W.; Calhoun, M. W.; Lemieux, L. J.; Puustinen, A.; Wikström, M.; Alben, J. O.; Gennis, R. B. *Biochemistry* **1994**, *33*, 13013−13021. (b) Brown, S.; Rumbley, J. N.; Moody, A. J.; Thomas, J. W.; Gennis, R. B.; Rich, P. R. *Biochim. Biophys. Acta* **1994**, *1183*, 521−532.

(7) Iwata, S.; Ostermeier, C.; Ludwig, B.; Michel, H. *Nature* **1995**, *376*, 660−669.

(8) Tsukihara, T.; Aoyama, H.; Yamashita, E.; Tomizaki, T.; Yamaguchi, H.; Shinzawa-Itoh, K.; Nakashima, R.; Yaono, R.; Yoshikawa, S. *Science* **1995**, *269*, 1069−1074.

(9) In the *Paracoccus denitrificans* structure,[7] the electron density map indicates the presence of solvent or (added) azide residing between the heme a_3 iron and Cu_B, which are 5.2 Å apart. Subunit I provides two His ligands to Cu_B (276 and 326), while His-325 appears not to be coordinated and is proposed to be intimately involved in the proton translocation process.[2a,7] In the bovine heart structure,[8] no bridging ligand is detected, the $Fe_{a3}\cdots Cu$ distance is 4.5 Å, and Cu_B directly coordinates all three His ligands (240, 290, and 291).

(10) (a) Varotsis, C.; Zhang, Y.; Appelman, E. H.; Babcock, G. T. *Proc. Natl. Acad. Sci. U.S.A.* **1993**, *90*, 237−241. (b) Ogura, T.; Takahashi, S.; Hirota, S.; Shinzawa-Itoh, K.; Yoshikawa, S.; Appelman, E. H.; Kitagawa, T. *J. Am. Chem. Soc.* **1993**, *115*, 8527−8536.

(11) Day, E. P.; Peterson, J.; Sendova, M. S.; Schoonover, J.; Palmer, G. *Biochemistry* **1993**, *32*, 7855−7860 and references cited therein.

(12) Wikström, M.; Morgan, J. E. *J. Biol. Chem.* **1992**, *267*, 10266−10273.

(13) Previously interpreted strong magnetic coupling in the heme a_3/Cu_B site appears to be inconsistent with the lack of bridging ligand and large heme $a_3\cdots Cu_B$ distances observed for the protein structures. See refs 7−9, 11, and the following: Gennis, R.; Ferguson-Miller, S. *Science* **1995**, *269*, 1063−1064.

(14) (a) Karlin, K. D.; Fox, S.; Nanthakumar, A.; Murthy, N. N.; Wei, N.; Obias, H. V.; Martens, C. F. *Pure Appl. Chem.* **1995**, *67*, 289−296. (b) Holm, R. H. *Pure Appl. Chem.* **1995**, *67*, 217−224. (c) Kitajima, N. *Adv. Inorg. Chem.* **1992**, *39*, 1−77. (d) Karlin, K. D. *Science* **1993**, *261*, 701−708.

(15) (a) Gunter, M. J.; Mander, L. N.; Murray, K. S. *J. Chem. Soc., Chem. Commun.* **1981**, 799−801. (b) Berry, K. J.; Gunter, M. J.; Murray, K. S. In *Oxygen and Life*; The Royal Society of Chemistry: London, U.K., 1980; Special Publication No. 39; pp 170−179. (c) Karlin, K. D.; Nanthakumar, A.; Fox, S.; Murthy, N. N.; Ravi, N.; Huynh, B. H.; Orosz, R. D.; Day, E. P. *J. Am. Chem. Soc.* **1994**, *116*, 4753−4763. (d) Nanthakumar, A.; Nasir, M. S.; Karlin, K. D.; Ravi, N.; Huynh, B. H. *J. Am. Chem. Soc.* **1992**, *114*, 6564−6566. (e) Collman, J. P.; Herrmann, P. C.; Boitrel, B.; Zhang, X.; Eberspacher, T. A.; Fu, L.; Wang, J.; Rousseau, D. L.; Williams, E. R. *J. Am. Chem. Soc.* **1994**, *116*, 9783−9784.

(16) (a) Gunter, M. J.; Mander, L. N.; Murray, K. S.; Clark, P. E. *J. Am. Chem. Soc.* **1981**, *103*, 6784−6787. (b) Chang, C. K.; Koo, M. S.; Ward, B. *J. Chem. Soc., Chem. Commun.* **1982**, *716*−719. (c) Bag, N.; Chern, S.-S.; Peng, S.-M.; Chang, C. K. *Inorg. Chem.* **1995**, *34*, 753−756. (d) Bulach, V.; Mandon, D.; Weiss, R. *Angew. Chem., Int. Ed. Engl.* **1991**, *30*, 572−575. (e) Giraudeau, A.; Gisselbrecht, J. P.; Gross, M.; Weiss, J. *J. Chem. Soc., Chem. Commun.* **1993**, 1103−1105. (f) Thomson, M. A.; Andersen, K. A.; Anderson, O. P.; Elliott, C. M. *Abstracts of Papers*, 205th National Meeting of the American Chemical Society: Denver, CO; American Chemical Society: Washington, DC, 1993; INOR 509. (g) Casella, L.; Monzani, E.; Gullotti, M.; Gliubich, F.; De Gioia, L. *J. Chem. Soc., Dalton Trans.* **1994**, 3203−3210.

Scheme 1

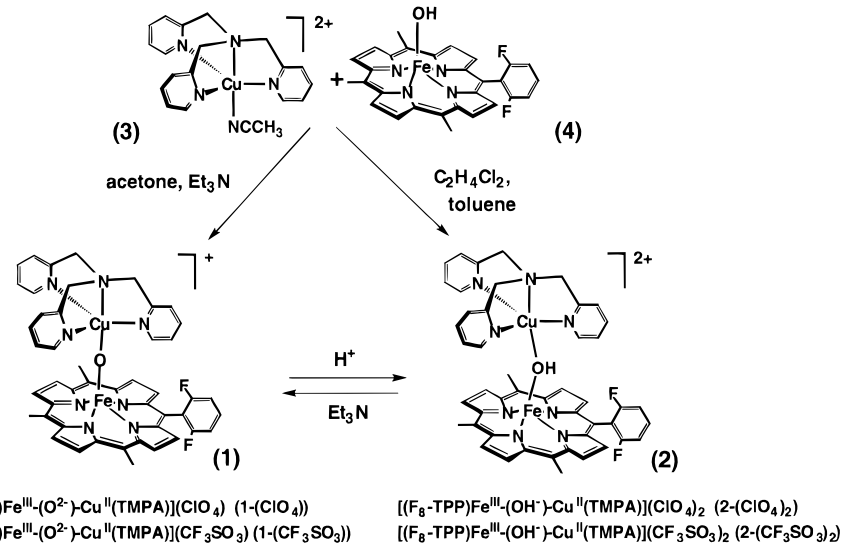

$Cu^{II}L$ complexes may represent species formed and responsible for cyanide poisoning,[18] while oxo- or hydroxo-bridged complexes could be enzyme "resting-state" models.[15a,b,16a,17,19] As other possible oxidized-state enzyme forms, there is also considerable interest in the chemistry of $Fe^{III}-Cu^{II}$ centers with ligand probes such as azide, formate, chloride, or even phenolate; some examples have been reported.[20]

Included in our own investigations are oxo- and hydroxo-bridged compounds $[(F_8\text{-TPP})Fe^{III}-(O^{2-})-Cu^{II}(TMPA)]^+$ (**1**) and $[(F_8\text{-TPP})Fe^{III}-(OH^-)-Cu^{II}-(TMPA)]^{2+}$ (**2**)[14a,15c,19,21] (Scheme 1). Complex **1** can form by the reaction of $[(TMPA)Cu^{I}(RCN)]^+$ with $(F_8\text{-TPP})Fe^{II}(pip)_2$ (pip = piperidine) or (F_8-TPP)Fe^{II} and dioxygen,[21] representing a crude heme-copper enzyme functional model. A detailed X-ray and electronic structural description of **1** has been published.[15c] Hydroxo complex **2** can be generated by protonation of **1**; addition of base to **2** gives back **1**.[19] An understanding of such acid−base interconversion chemistry is of potential importance, since the heme-copper center is the site of ("scalar") proton transfer to O_2-derived O atoms, as well as ("vectorial") H^+ ion translocation across the membrane. The molecular mechanism of proton pumping[2,7] has been suggested to involve protonation−deprotonation and deligation−ligation changes of the ligands bound to Cu or Fe at the heme-Cu center; indeed Fe−O(H)−Cu intermediates have been speculated to be involved.[2a]

This report emphasizes the relationship between μ-oxo **1** and μ-hydroxo **2**, detailing syntheses from LCu^{II} and PFe^{III} precursors **3** and **4** (Scheme 1), reversible protonation chemistry, and comparisons of structure and physical properties. Furthermore, we utilize XAS to provide a detailed picture of the structure of **2**, while also comparing the results to XAS properties of **1** and to the quinol oxidase aa_3-600 from *Bacillus subtilis*.

Experimental Section

Materials and Methods. Reagents and solvents used were of commercially available reagent quality unless otherwise stated. Dichloromethane (CH_2Cl_2) was stirred with concentrated sulfuric acid for several days and washed with water, sodium carbonate (10%) solution, and water. It was then dried over anhydrous $MgSO_4$ and CaH_2 before a final reflux and distillation from CaH_2. Acetonitrile (CH_3CN) was distilled from CaH_2. Anhydrous diethyl ether was prepared by passing reagent-grade solvent through a column of activated alumina. Preparation and handling of air-sensitive materials was carried out under an argon atmosphere using standard Schlenk techniques. Solid samples were stored and transferred, and samples for IR and NMR spectra were prepared, in a Vacuum Atmospheres inert atmosphere glovebox filled with nitrogen.

Elemental analyses were performed by National Chemical Consulting, Tenafly, NJ, and Desert Analytics, Tucson, AZ. Infrared spectra were recorded as Nujol mulls on a Mattson Galaxy Series 4030 FTIR spectrometer. UV−vis spectra were recorded on a Shimadzu UV 160U instrument or a Hewlett-Packard 8452A diode array spectrometer driven by a Compaq Desk Pro 386S computer using software written by On-Line Instrument Systems, Inc. (Bogart, GA). ^{1}H NMR spectra were obtained at 300 MHz on a Bruker AMX-300 instrument. Chemical shifts are reported as δ values downfield from an internal standard of Me_4Si.

[(TMPA)Cu^{II}(CH_3CN)](ClO_4)$_2$ [3-(ClO_4)$_2$]. In a 125 mL Erlenmeyer flask equipped with a stir bar was dissolved TMPA[22] (1.00 g, 3.44 mmol) in CH_3CN (20 mL). To this solution was added $Cu(ClO_4)_2\cdot 6H_2O$ (1.159 g, 3.127 mmol). An immediate sky-blue solution developed, which was stirred for 15 min and filtered by gravity (coarse frit) into another 125 mL Erlenmeyer flask, and the mother flask was rinsed with CH_3CN (5 mL). To the combined filtrate was added ether (∼20 mL), through the frit, until the cloud point; the flask was then covered with Parafilm and stored at −20 °C. After 2 h, some blue crystals had deposited; another aliquot of ether (10 mL) was added, and the flask was covered and allowed to stand at 25 °C. The next day, ether (10 mL) was added as before to the solution and crystals, and this was allowed to stand again. This process was repeated one more time until the supernatant was virtually colorless; the blue plates were collected on a coarse frit, washed with ether (10 mL), and dried *in vacuo* for 48 h to give 1.65 g (89%) of product. Anal. Calcd for $C_{20}H_{21}N_5CuCl_2O_8$: C, 40.45; H, 3.56; N, 11.79. Found: C, 40.20; H, 3.53; N, 11.51. UV−vis (CH_3CN): 861 (ϵ = 250 M^{-1} cm^{-1}) nm.

[(F_8-TPP)Fe−O−Cu(TMPA)](ClO_4) [1-(ClO_4)]. In a 100 mL Schlenk flask equipped with a stir bar was dissolved [(F_8-TPP)Fe−(OH)−Cu(TMPA)]$(ClO_4)_2\cdot C_7H_8$ (0.294 g, 0.2 mmol) in deaerated acetone (20 mL) to yield a reddish solution. To this was added NEt_3

(17) (a) Scott, M. J.; Zhang, H. H.; Lee, S. C.; Hedman, B.; Hodgson, K. O.; Holm, R. H. *J. Am. Chem. Soc.* **1995**, *117*, 568−569. (b) Lee, S. C.; Holm, R. H. *J. Am. Chem. Soc.* **1993**, *115*, 11789−11798.

(18) (a) Scott, M. J.; Holm, R. H. *J. Am. Chem. Soc.* **1994**, *116*, 11357−11367. (b) Gunter, M. J.; Berry, K. J.; Murray, K. S. *J. Am. Chem. Soc.* **1984**, *106*, 4227.

(19) Nanthakumar, A.; Fox, S.; Murthy, N. N.; Karlin, K. D.; Ravi, N.; Huynh, B. H.; Orosz, R. D.; Day, E. P.; Hagen, K. S.; Blackburn, N. J. *J. Am. Chem. Soc.* **1993**, *115*, 8513−8514.

(20) (a) Gunter, M. J.; Mander, L. N.; McLaughlin, G. M.; Murray, K. S.; Berry, K. J.; Clark, P. E.; Buckingham, D. A. *J. Am. Chem. Soc.* **1980**, *102*, 1470−1473. (b) Berry, K. J.; Clark, P. E.; Gunter, M. J.; Murray, K. S. *Nouv. J. Chim.* **1980**, *4*, 581−585.

(21) Nanthakumar, A.; Fox, S.; Karlin, K. D. *J. Chem. Soc., Chem. Commun.* **1995**, 499−501.

(22) Tyeklár, Z.; Jacobson, R. R.; Wei, N.; Murthy, N. N.; Zubieta, J.; Karlin, K. D. *J. Am. Chem. Soc.* **1993**, *115*, 2677−2689.

(28 μL, 0.2 mmol) via syringe, in one shot; an immediate color change to bright red was observed. The solution was then concentrated *in vacuo* to about half the original volume and allowed to stand. After 2 days, a copious red precipitate was collected on a coarse frit, washed quickly with acetone (5 mL), and dried *in vacuo* for 48 h to give 0.174 g (68%) of red microcrystalline solid. Anal. Calcd for $C_{62}H_{38}N_8FeCuClO_5F_8$: C, 58.08; H, 2.99; N, 8.74. Found: C, 58.37; H, 3.06; N, 8.39. ^{1}H NMR (CD_3CN): δ 65.7 (v br, pyrrole, 8 H), 9.6, 9.2 (*m*-phenyl, 8 H), 7.9 (*p*-phenyl, 4 H), 4.7 (py4 of TMPA, 3H), −6.8 (py5 of TMPA, 3 H), −21.6 (py3 of TMPA, 3H), −104 (CH_2 of TMPA, 6 H) ppm.

[(F_8-TPP)Fe−(OH)−Cu(TMPA)](ClO$_4$)$_2$·C_7H_8 [2-(ClO$_4$)$_2$]. In a 100 mL Schlenk flask equipped with a stir bar were charged the solids (F_8-TPP)Fe−OH[15c] (0.166 g, 0.2 mmol) and powdered [Cu(TMPA)(CH_3-CN)](ClO$_4$)$_2$ (0.119 g, 0.2 mmol). These were stirred *in vacuo* for 1 h to effect intimate mixing; deaerated $C_2H_4Cl_2$ (25 mL) was then introduced to generate an immediate brown-red solution. After stirring for 30 min, deaerated C_7H_8 (15 mL) was added, the solution filtered through a medium frit into another 100 mL Schlenk flask, and the solution stored at −20 °C. On the next day, a crop of black plates was collected on a coarse frit, washed with toluene (10 mL), and dried *in vacuo* for 48 h to give 0.222 g (75%) of product. Anal. Calcd for $C_{69}H_{47}O_9F_8N_8Cl_2CuFe$: C, 56.20; H, 3.21; N, 7.60. Found: C, 56.10; H, 3.20; N, 7.55. UV−vis (CH_2Cl_2): 408 nm (ϵ = 106 000 M^{-1} cm^{-1}), 572 nm (ϵ = 9900 M^{-1} cm^{-1}). ^{1}H NMR (CD_2Cl_2): δ 69 (v br, pyrrole), 11.5, 10.7 (*m*-phenyl, 8 H), 7.6 (*p*-phenyl, 4 H), 7.2 ($C_6H_5CH_3$, 5 H), 2.3 ($C_6H_5CH_3$, 3 H) ppm.

[(TMPA)Cu^{II}(CF$_3$SO$_3$)](CF$_3$SO$_3$)·H$_2$O [3-(CF$_3$SO$_3$)$_2$]. In the dry box, copper(II) triflate (1.00 g, 2.76 mmol) was added into a 100 mL Schlenk flask equipped with a stir bar. On the Schlenk line, under argon, was added TMPA (0.871 g, 3.00 mmol); the addition of deaerated CH_3CN (30 mL) to the stirred solids yielded an immediate sky-blue solution. Stirring was maintained for 30 min; then, in air, ether was added to the cloud point (∼50 mL). The solution was then allowed to filter by gravity (coarse frit) into an Erlenmeyer flask (250 mL), which was subsequently covered with Parafilm and stored at −20 °C. On the next day, a crop of beautiful blue parallelepipeds was collected by filtration (coarse frit), washed with ether (20 mL), and dried *in vacuo* to yield 1.682 g (91%) of product. Anal. Calcd for $C_{20}H_{20}O_7F_6N_4S_2Cu$: C, 35.85; H, 3.01; N, 8.36; F, 17.01. Found: C, 35.70; H, 3.02; N, 8.27; F, 16.96. UV−vis (CH_3CN): 857 nm (ϵ = 240 M^{-1} cm^{-1}).

[(F_8-TPP)Fe−O−Cu(TMPA)](CF$_3$SO$_3$) [1-(CF$_3$SO$_3$)]. In a 100 mL Schlenk flask equipped with a stir bar were charged the solids (F_8-TPP)Fe−OH (**4**) (0.166 g, 0.2 mmol) and [Cu^{II}(TMPA)(CF_3-SO_3)](CF$_3$SO$_3$)·H_2O [**3**-(CF$_3$SO$_3$)$_2$] (0.136 g, 0.2 mmol). These were stirred for 30 min *in vacuo* to effect intimate mixing; then deaerated acetone (15 mL) was introduced. A red solution was generated, to which was promptly added NEt_3 (28 μL, 0.2 mmol), in one shot, via syringe. A distinct color change, to a bright red, ensued; the volume of the solution was then reduced *in vacuo* to ∼10 mL, and the solution was allowed to stand under argon. After 2 days, a red precipitate had formed; this was collected on a coarse frit, washed with acetone (5 mL), and dried *in vacuo* for 48 h to give 0.188 g (71%) of red microcrystalline product. Anal. Calcd for $C_{63}H_{38}O_4F_{11}N_8SCuFe$: C, 56.83; H, 2.87; N, 8.41. Found: C, 57.13; H, 3.22; N, 7.85. ^{1}H NMR (acetone-d_6): δ 65.7 (v br, pyrrole, 8 H), 9.6, 9.2 (*m*-phenyl, 8 H), 7.9 (*p*-phenyl, 4 H), 4.7 (py4 of TMPA, 3H), −6.8 (py5 of TMPA, 3 H), −21.6 (py3 of TMPA, 3H), −98.9 (CH_2 of TMPA, 6 H) ppm.

[(F_8-TPP)Fe−(OH)−Cu(TMPA)](CF$_3$SO$_3$)$_2$ [2-(CF$_3$SO$_3$)$_2$]. In a 100 mL Schlenk flask equipped with a stir bar was charged **1**-(CF_3-SO_3) (0.133 g, 0.1 mmol). Deaerated $C_2H_4Cl_2$ (12 mL) was added to yield a bright red solution; with stirring, CF_3SO_3H (8.8 μL, 0.1 mmol) was introduced via syringe under argon. Deaerated toluene (∼25 mL) was added to the resulting brown-red solution, and this was then filtered through a medium frit into a 100 mL Schlenk flask and stored at −20 °C. On the next day, a copious sparkling solid was collected on a coarse frit, washed with toluene (10 mL), and dried *in vacuo* for 48 h to give 0.104 g (75%) of black crystalline product. Anal. Calcd for $C_{64}H_{39}O_7F_{14}N_8S_2CuFe$: C, 51.88; H, 2.65; N, 7.56. Found: C, 51.74; H, 2.64; N, 7.64. ^{1}H NMR (CD_2Cl_2): δ 71.5 (v br, pyrrole), 11.5, 10.7 (*m*-phenyl, 8 H), 7.6 (*p*-phenyl, 4 H) ppm.

Evans Method NMR Experiments. The ambient temperature (298 K) magnetic moment of **2**-(ClO$_4$)$_2$ was measured by the Evans method.[23] In the coaxial tube configuration, the inner capillary contained solvent (CD_2Cl_2, 2% TMS) with the outer 5 mm tube also containing dissolved **2**-(ClO$_4$)$_2$. The frequency difference between the TMS reference signals was measured (300 MHz instrument) to be $\Delta\nu$(**2**) = 72 Hz. Triethylamine (1 equiv) was added to convert **2**-(ClO$_4$)$_2$ to **1**-(ClO$_4$), which was confirmed by the change in the pyrrole proton signal from 68.5 ppm for **2**-(ClO$_4$)$_2$ to 65 ppm for **1**-(ClO$_4$). The frequency difference between TMS signals was now $\Delta\nu$(**1**) = 60.9 Hz. Assuming only small changes in χ_D (molar diamagnetic susceptibility) and molecular weights for **1**-(ClO$_4$) and **2**-(ClO$_4$)$_2$, the molar paramagnetic susceptibility χ_M is related to $\Delta\nu$ by the equation χ_M(**2**)/χ_M(**1**) = $\Delta\nu$(**2**)/$\Delta\nu$(**1**). Since μ_B (= 5.1 at 298 K) and hence the molar susceptibility for compound **1**-(ClO$_4$) is known accurately,[15c] μ_B for **2**-(ClO$_4$)$_2$ was calculated as 5.5 ± 0.1. This *in situ* measurement allowed for a direct comparison with well-characterized **1**-(ClO$_4$) under identical conditions of concentration.

NMR Titration. Protonation of 1-(ClO$_4$). In the glovebox, a solution of **1**-(ClO$_4$) (∼0.013 g, 0.01 mmol) in CD_2Cl_2 (1 mL) was prepared and transferred to an NMR tube, and the ^{1}H NMR spectrum recorded. CF_3SO_3H (0.3 μL, 0.033 mmol), from a freshly opened ampule (Aldrich), was then introduced via a 1 μL syringe, the solution recapped and shaken, and the ^{1}H NMR spectrum recorded. This process of adding aliquots of acid and recording spectra was performed twice more, to attain the titration "end-point".

EXAFS Data Collection and Analysis. EXAFS data were collected at the National Synchrotron Light Source (NSLS), Brookhaven National Laboratory, and at the Stanford Synchrotron Radiation Laboratory (SSRL). Experimental conditions are summarized in a table in the supporting information. Perchlorate salts of **1** and **2** were measured as powders in the transmission mode. Because of the relatively high molecular weight of these complexes, they were not diluted with boron nitride. Samples of the dioxygen complex [{(TMPA)Cu^{II}}$_2$(O$_2$)](ClO$_4$)$_2$ [**5**-(ClO$_4$)$_2$] were measured as frozen glasses in dichloromethane at 100 K in the fluorescence mode using a 13-element Ge detector. The protein samples were measured as frozen glasses in 20% glycerol at 11−14 K in the fluorescence mode also using a 13-element Ge detector. To avoid detector saturation, the count rate of each detector channel was kept below 35 KHz, by adjusting the hutch entrance slits, or by moving the detector in or out from the cryostat windows. Under these conditions, no dead-time correction was necessary. The summed data for each detector was then inspected, and only those channels that gave high-quality backgrounds free from glitches, dropouts, or scatter peaks were included in the final average.

Raw data were averaged, background subtracted, and normalized to the smoothly varying background atomic absorption using the EXAFS data reduction package EXAFSPAK (Graham George, 1990). Data analysis was carried out by least-squares curve fitting utilizing full curved-wave calculations as formulated by the SRS library program EXCURV,[24] using methodology previously described in detail.[25] For single-scattering (two-body) pathways, the parameters refined in the fit were as follows: E_0, the photoelectron energy threshold; R_i, the distance from Cu or Fe to atom *i*; and $2\sigma^2_i$, the Debye−Waller term for atom *i*. Multiple-scattering (MS) (three-body) EXAFS contributions were included for Cu−O−Fe and Fe−N_α−C_γ (porphyrin) pathways using well-documented methodology also described in previous papers from this laboratory.[25] In the MS simulations, the adjustable parameters were M−X and M−Y distances and MXY angle, where M is the absorber and X and Y are the scattering atoms of the three-body pathway. The quality of the fits was determined using a least-squares

(23) (a) Evans, D. F. *J. Chem. Soc.* **1959**, 2003. (b) Bartle, K. D.; Dale, B. J.; Jones, D. W.; Maricic, J. *J. Magn. Reson.* **1973**, *12*, 286.

(24) (a) Binsted, N.; Gurman, S. J.; Campbell, J. W. *Daresbury Lab. EXCURV88 Program* **1988**. (b) Gurman, S. J. In *Synchrotron Radiation and Biophysics*; Hasnain, S. S., Ed.; Ellis Horwood Ltd.: Chichester, U.K., 1989; pp 9−42. (c) Gurman, S. J.; Binsted, N.; Ross, I. *J. Phys. C* **1984**, *17*, 143−151. (d) Gurman, S. J.; Binsted, N.; Ross, I. *J. Phys. C* **1986**, *19*, 1845−1861.

(25) (a) Strange, R. W.; Blackburn, N. J.; Knowles, P. F.; Hasnain, S. S. *J. Am. Chem. Soc.* **1987**, *109*, 7157−7162. (b) Blackburn, N. J.; Hasnain, S. S.; Pettingill, T. M.; Strange, R. W. *J. Biol. Chem.* **1991**, *266*, 23120−23127. (c) Sanyal, I.; Karlin, K. D.; Strange, R. W.; Blackburn, N. J. *J. Am. Chem. Soc.* **1993**, *115*, 11259−11270.

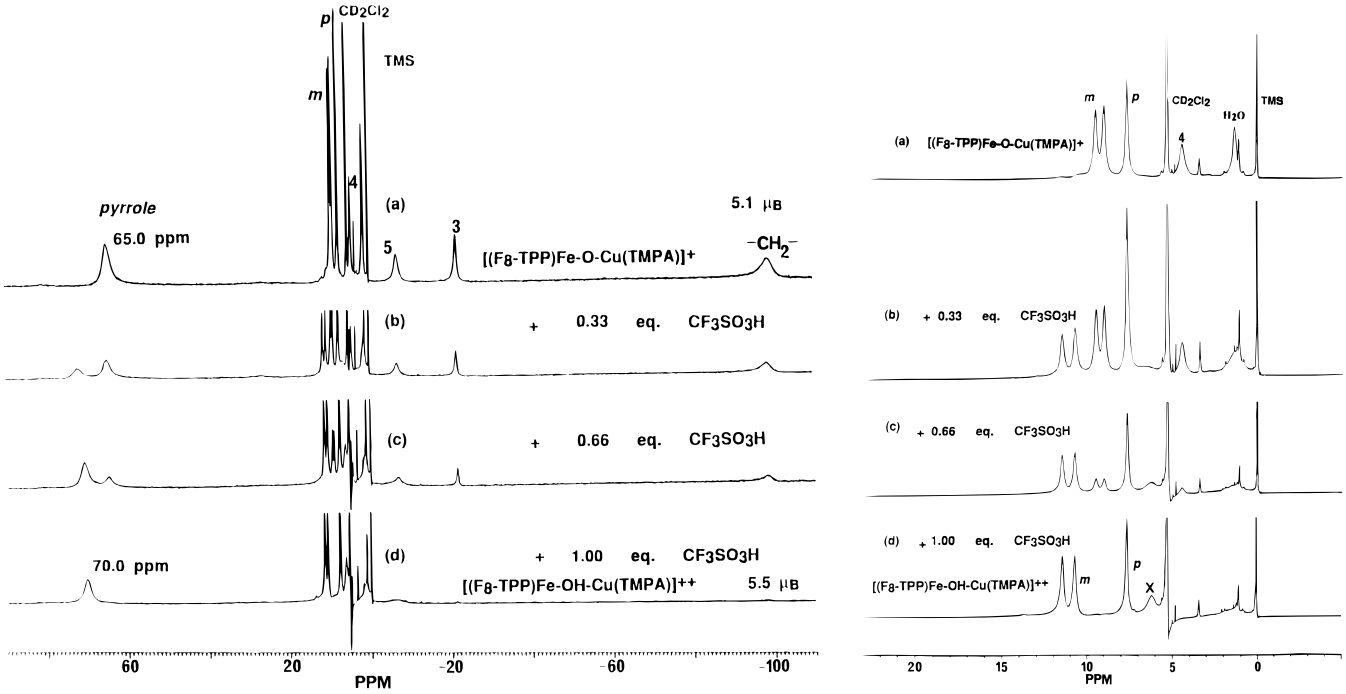

Figure 2. Left: Effect on the ^{1}H-NMR spectrum of adding protons (triflic acid) to [(F_8-TPP)Fe^{III}−(O^{2-})−Cu^{II}(TMPA)](ClO_4) [**1**-(ClO_4)]: (a) spectrum of **1**-(ClO_4), (b) after adding 0.33 equiv of CF_3SO_3H, (c) after adding 0.66 equiv of CF_3SO_3H, (d) after adding 1.00 equiv of CF_3SO_3H producing [(F_8-TPP)Fe^{III}−(OH^-)−Cu^{II}(TMPA)]$^{2+}$ (**2**) (CD_2Cl_2 solvent, spectrometer frequency 300 MHz, 298 K). Peaks labeled 3, 4, and 5 represent proton NMR signals due to the respective pyridyl ring positions of the TMPA moiety of **1**-(ClO_4), −CH_2− represents the absorption due to the methylene protons of TMPA, and *m* and *p* represent the signals due to the meta and para phenyl protons of the porphyrin ring. Inset, right: ^{1}H-NMR spectrum of **1**-(ClO_4), showing the expanded region 0−20 ppm. X represents a ^{1}H-NMR signal due to 4-pyridyl protons of the TMPA moiety of **2**.

fitting parameter, *F*, defined as $F^2 = (1/N)\sum k^6(\chi_i^{\text{theor}} - \chi_i^{\text{exp}})^2$, referred to as the fit index.

Results and Discussion

Synthesis. The emphasis here is to detail the acid−base syntheses and properties of μ-oxo complex **1** and the related conjugate acid dicationic form [(F_8-TPP)Fe^{III}−(OH^-)−Cu^{II}(TMPA)]$^{2+}$ (**2**), Scheme 1. Holm and co-workers[17] have also generated similar types of model compounds, a μ-oxo complex [(OEP)Fe^{III}−O−Cu^{II} (Me_6tren)]$^+$ [OEP = octaethylporphyrinate; Me_6tren = tris[2-(*N*,*N*-dimethylamino)ethyl]amine] and an independently synthesized μ-hydroxo species [(OEP)Fe^{III}−(OH^-)−Cu^{II} (Me_5dien)($OClO_3$)]$^+$ (Me_5dien = 1,1,4,5,5-pentamethyldiethylenetriamine).

Complexes **1** and **2** were prepared using both perchlorate and triflate anions. Pentacoordinate [(TMPA)Cu^{II}(CH_3CN)]$^{2+}$ (**3**)[26] is a convenient synthetic precursor because of its labile acetonitrile ligand. Thus, μ-oxo complex **1**-(ClO_4) was prepared *via* the acid−base reaction of [(TMPA)Cu^{II}(CH_3CN)][ClO_4]$_2$ [**3**-(ClO_4)$_2$] and (F_8-TPP)Fe^{III}−OH (**4**) with Et_3N in CH_3CN (Scheme 1),[19] and the triflate analog, **1**-(CF_3SO_3), was prepared in a like manner.

The hydroxo complex **2** can be prepared by two routes (Scheme 1). In the first, Et_3N is left out when reacting **3** and **4**. The second route is to directly protonate the oxo complexes. Addition of CF_3SO_3H (1 equiv) to **1**-(CF_3SO_3) in CH_2Cl_2 gave an immediate color change from bright red to red-brown. Subsequent addition of toluene precipitated black crystalline μ-hydroxo complex [(F_8-TPP)Fe−(OH^-)−Cu(TMPA)](CF_3SO_3)$_2$ [**2**-(CF_3SO_3)$_2$]. This complex was also prepared by combination of equimolar amounts of **4** and [(TMPA)Cu(CH_3CN)](CF_3SO_3)$_2$ [**3**-(CF_3SO_3)$_2$] in 1,2-dichloroethane/toluene.

(26) Jacobson, R. R. Ph.D. Thesis, State University of New York at Albany, 1989.

To complete the picture, we wished to prove we could synthetically generate oxo complexes [(F_8-TPP)Fe^{III}−(O^{2-})−Cu^{II}(TMPA)]$^+$ (**1**) by *deprotonation* of [(F_8-TPP)Fe^{III}−(OH^-)−Cu^{II}(TMPA)]$^{2+}$ (**2**). Thus, addition of 1 equiv of Et_3N in acetone to **2**-(ClO_4)$_2$ [prepared by combination of **3**-(ClO_4)$_2$ and **4**] gave **1**-(ClO_4) in 68% yield. Where the μ-oxo complex **1** is quite moisture sensitive and decomposes instantly, for example, in unpurified CH_2Cl_2, the μ-hydroxo moieties of **2** are relatively stable (i.e., for hours). Addition of >1 equiv of strong acid (CF_3SO_3H) in the protonation reaction, however, leads to immediate decomposition as witnessed from ^{1}H-NMR spectroscopy. Notably, the μ-hydroxo species also loses integrity, albeit slowly, in "dry" CH_3CN and acetone to yield the μ-oxo iron−porphyrin dimer [(F_8-TPP)Fe^{III}−(O^{2-})−Fe^{III}(F_8-TPP)][15c] and μ-oxo complex **1**, respectively.

Protonation Titration. Figure 2 shows the clean transformation of [(F_8-TPP)Fe^{III}−(O^{2-})−Cu^{II}(TMPA)](ClO_4) [**1**-(ClO_4)] to [(F_8-TPP)Fe^{III}−(OH^-)−Cu^{II}(TMPA)]$^{2+}$ (**2**) upon titration with CF_3SO_3H, added in increments of $^1/_3$ equiv (Experimental Section). In

$$\underset{\mathbf{1}}{[(F_8\text{-TPP})Fe-(O^{2-})-Cu(TMPA)]^+} + H^+ \rightarrow \underset{\mathbf{2}}{[(F_8\text{-TPP})Fe-(OH^-)-Cu(TMPA)]^{2+}}$$

the downfield region, the 65 ppm absorption, assigned to the eight pyrrole hydrogens of the F_8-TPP porphyrinate ligand,[15c] decreases in intensity as a new peak at 70 ppm grows.[27] The assignment of the latter resonance was confirmed by ^{2}H-NMR spectroscopy of **2**, prepared with deuteriated pyrrole.[15c] We

(27) This chemical shift is incompatible with species such as (P)Fe^{III}−triflate (~53 ppm) or (P)Fe^{III}−perchlorate (~20 ppm), which one might conceive as alternative reaction products.

note that this pyrrole absorption occurs at 68.5 ppm for [(F_8-TPP)Fe^{III}−(OH^-)−Cu^{II}(TMPA)](ClO_4)$_2$ [**2**-(ClO_4)$_2$] and 71 ppm for [(F_8-TPP)Fe^{III}−(OH^-)−Cu^{II}(TMPA)](CF_3SO_3)$_2$ [**2**-(CF_3SO_3)$_2$]; thus the mixed-anion species generated in our titration from **1**-(ClO_4) plus CF_3SO_3H gives an intermediate chemical shift. This anion dependence may be caused by H bonding with the OH^- hydrogen atom. We suggest this in light of observations made for [(OEP)Fe^{III}−(OH^-)−Cu^{II}(Me_5dien)($OClO_3$)]$^+$; this displays a coordinated perchlorate intramolecularly hydrogen bonded to the μ-OH^-, where the ∠Fe−(OH)−Cu angle varied from 157.0(2)° to 163.1(4)° according to the crystallization conditions and nature of the counterion, i.e., ClO_4^- or SbF_6^-.[17a]

Other peaks in the ^{1}H-NMR spectrum of **1** also change upon titration (Figure 2 inset, b-d); new downfield shifted "doublet" *m*-phenyl porphyrinate resonances grow in. There is no shift of the 7.8 ppm absorption on conversion of **1** to **2**, typical of the *p*-phenyl position of iron(III) tetraarylporphyrinates. The upfield-shifted peaks are associated with the protons of the TMPA moiety[15c,28] and disappear upon conversion to **2** at this temperature (Figure 2 inset, a−d). The complete conversion of μ-oxo complex **1** to the μ-hydroxo-bridged complex **2** with the addition of exactly 1 equiv of acid indicates the strongly basic nature of the bridging oxo ligand of **1** (*vide infra*).

Magnetic Properties. The ^{1}H-NMR spectra contain information relevant to spin and oxidation states, as well as magnetic coupling in these compounds. While typical high-spin (TPP)-Fe^{III}−X (X = Cl^-, F^-, OH^-) compounds exhibit a pyrrole resonance at ∼80 ppm,[29] the diminished shift in [(F_8-TPP)Fe^{III}−(O^{2-})−Cu^{II}(TMPA)]$^+$ (**1**) (i.e., 65 ppm) can be accounted for by the antiferromagnetic coupling to Cu(II), which gives rise to an $S = 2$ system.[15c] The downfield shifting to ∼70 ppm in [(F_8-TPP)Fe^{III}−(OH^-)−Cu^{II} (TMPA)]$^{2+}$ (**2**) therefore suggests weaker coupling here, which is confirmed by determination of room-temperature magnetic moments for **1** and **2**. For **1**, variable-temperature multifield saturation magnetization studies indicate an $\mathbf{S} = 2$ system with $J = -87$ cm^{-1} (based on a Hamiltonian for antiferromagnetic coupling ($-2J\boldsymbol{S}_1\cdot\mathbf{S}_2$)), and the room-temperature magnetic moment is 5.1 ± 0.1 μ_B both in solution and the solid state.[15c] A similar study has proven not to be possible for **2**, but μ_B could be accurately measured here by conversion of **2** to **1** (by adding Et_3N) in an *in situ* Evans NMR method experiment, giving a value of 5.5 ± 0.1 μ_B. These values are considerably reduced from the spin-only value of 6.2 μ_B expected for a completely uncoupled high-spin Fe(III)−Cu(II) system [which is observed for [(OEP)Fe^{III}−(F^-)−Cu^{II} (ligands)]$^+$][17b] and still diminished from the expected spin-only value for high-spin Fe(III) (5.9 μ_B). This clearly suggests that the implicit antiferromagnetic coupling in (P)Fe^{III}−X−Cu^{II}L is of lesser magnitude for X = OH^- (**2**) versus X = O^{2-} (**1**). This attenuation of coupling upon protonation is also illustrated by [(OEP)Fe^{III}−(O^{2-})−Cu^{II}−(Me_6tren)]$^+$ and [(OEP)-Fe^{III}−(OH^-)−Cu^{II} (Me_5dien)($OClO_3$)]$^+$, for which $J > -200$ cm^{-1} (5.03 μ_B at room temperature) and $J \approx -80$ cm^{-1}, respectively;[17] note that the absolute value of the coupling is greater in the OEP-containing complexes, which probably reflects differences in the ligands for copper and porphyrinates used.

Slow Proton Exchange and Implied Structural Consequences. Another significant aspect concerning the ^{1}H-NMR spectrum of [(F_8-TPP)Fe^{III}−(O^{2-})−Cu^{II}(TMPA)]$^+$ (**1**) is that the protonation process is slow on the NMR time scale (300 MHz). This is deduced from the observation of two distinctive sets of resonances in mixtures of **1** and [(F_8-TPP)Fe^{III}−(OH^-)−Cu^{II}(TMPA)]$^{2+}$ (**2**) (Figure 2 and inset, b, c), also seen over a wide temperature range. If protonation were rapid, only one (averaged) resonance would be observed. Apparently, oxo-bridged metal ion species are predisposed to relatively slow protonation reactions.[30] For example, protonation of one oxo bridge in the bis(μ-oxo)−dimanganese(III) complex {[(6-methylbispicen−Mn^{III}(μ-O)]$_2$}$^{2+}$ (6-methylbispicen = *N,N′*-bis-[(6-methylpyrid-2-yl)ethane-1,2-diamine] in MeCN solvent occurs with $k_{H^+} = 5440$ M^{-1} s^{-1} where $\log_{10}(K_{eq}) = 16.2$.[31]

Perhaps of more direct relevance for the present study is the observation that (OEP)Fe^{III}−(O^{2-})−Fe^{III}(OEP) protonates with $k_{H^+} = 12\,700$ M^{-1} s^{-1} at −10 °C;[30] a crystal structure[32] reveals a bending from 172° in the parent oxo-bridged complex to 146° in the hydroxo-bridged product [(OEP)Fe^{III}−(OH^-)−Fe^{III}-(OEP)]$^+$. Norton and co-workers have ascribed such slow

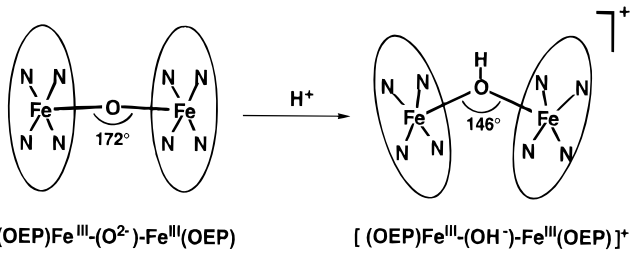

protonation to the requirement for disruption of oxo-to-metal π-backbonding and necessary rehybridization;[30,31] i.e., the extensive geometric and electronic rearrangement leads to large kinetic barriers. In addition, such protonations typically result in increased metal−oxygen bond distances, ∼0.1 Å.[30,33] The observations of slow protonation of [(F_8-TPP)Fe^{III}−(O^{2-})−Cu^{II}-(TMPA)]$^+$ (**1**) and weaker magnetic coupling (which would be expected with bond lengthening and bridge bending) thus leads us to propose that **2** possesses a bent Fe−(OH)−Cu structure. This assertion is supported by the XAS studies described below.

Slow protonation may have relevance to heme-copper oxidase function. Both Fe^{III}−(O^{2-})−Cu^{II} and Fe^{III}−(OH^-)−Cu^{II} species have been considered as possible intermediates in the catalytic cycle of O_2 reduction and proton pumping occurring at the heme-Cu center.[2a] Proton transfers have been suggested to be slow, at least for certain steps in the overall reaction, and this may be important in order to allow near-steady-state concentrations of intermediates to accumulate during turnover.[2a,b,10a,30,34] As an aside, in non-heme iron[35] and manganese chemistries,[33] proton-dependent or proton-triggered metal reductions have also been proposed.

Estimated pK_a of [(F_8-TPP)Fe^{III}−(OH^-)−Cu^{II}(TMPA)]$^{2+}$ (2). We have also probed the acid−base interconversion equilibrium of μ-oxo **1** and μ-OH^- **2**. Monitoring the characteristic pyrrole resonances by ^{1}H-NMR spectroscopy in both CD_3CN and CD_2Cl_2, we find that complete and clean conversion of **1** (e.g., $\delta_{pyrrole} = 65.6$ ppm in CD_3CN) to **2** ($\delta_{pyrrole} = 74.9$

(28) A separate paper will provide details of definitive assignments of these peaks, by site-specific methylation and/or deuteriation experiments, and will describe temperature dependencies, likely mechanism of coupling, spin-delocalization, and NMR properties of mononuclear copper(II) complexes. Nanthakumar, A.; Fox, S.; Murthy, N. N.; Karlin, K. D. Manuscript in preparation.

(29) Goff, H. M. In *Iron Porphyrins*; Lever, A. B. P., Gray, H. B., Eds.; Addison-Wesley: Reading, MA, 1983; Part 1, Chapter 4.

(30) Kramarz, K. W.; Norton, J. R. *Prog. Inorg. Chem.* **1994**, *42*, 1−65.
(31) Carroll, J. M.; Norton, J. R. *J. Am. Chem. Soc.* **1992**, *114*, 8744−8745.
(32) Scheidt, W. R.; Cheng, B.; Safo, M. K.; Cukiernik, F.; Marchon, J.-C.; Debrunner, P. G. *J. Am. Chem. Soc.* **1992**, *114*, 4420−4421.
(33) Baldwin, M. J.; Stemmler, T. L.; Riggs-Gelasco, P. J.; Kirk, M. L.; Penner-Hahn, J. E.; Pecoraro, V. L. *J. Am. Chem. Soc.* **1994**, *116*, 11349−11356.
(34) Hallén, S.; Nilsson, T. *Biochemistry* **1992**, *31*, 11853−11859.
(35) Kurtz, D. M., Jr. *Chem. Rev.* **1990**, *90*, 585−606.

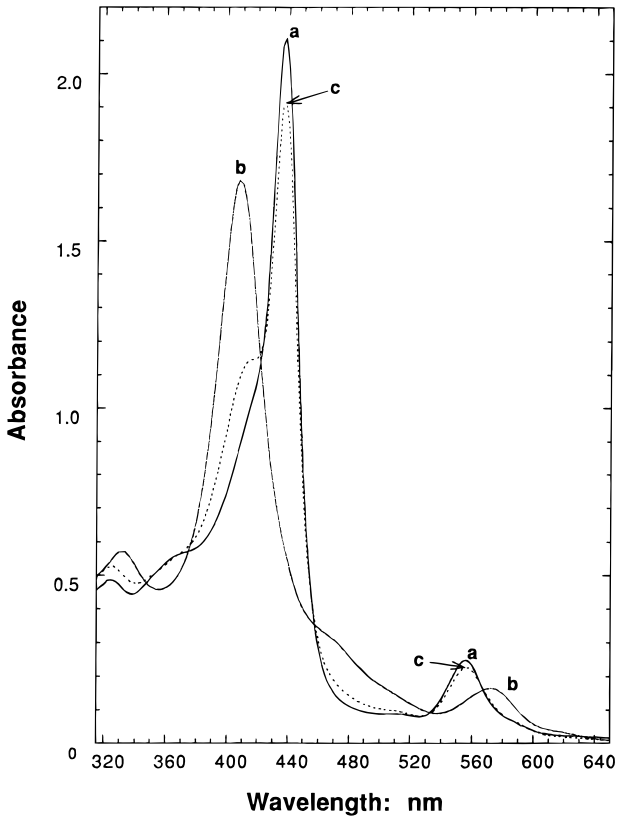

Figure 3. Reversible acid−base interconversion of $[(F_8\text{-TPP})Fe^{III}-(O^{2-})-Cu^{II}(TMPA)]^+$ (**1**) and $[(F_8\text{-TPP})Fe^{III}-(OH^-)-Cu^{II}(TMPA)]^{2+}$ (**2**), as monitored by UV−visible spectroscopy: (a) **1**-(ClO_4) (λ_{max} = 436, 554 nm; 1.59×10^{-5} M); (b) after addition of ∼1 equiv of triflic acid (0.15 μL of 1.14 M solution), λ_{max} = 408, 572 nm, identical to the spectrum of authentic μ-OH^- compound **2**; (c) after addition of ∼1 equiv of base (0.22 μL of 0.718 M NEt_3). The absorbance intensity of the Soret band corresponds to ∼90% conversion from **2** to **1**. Methylene chloride solvent, 298 K.

ppm) occurs when using 2,4-lutidinium triflate ($LuH^+CF_3SO_3^-$), or stronger protic acids (e.g., anilinium perchlorate). However, no change occurred when trimethylammonium tetraphenylborate ($Me_3NH^+Ph_4B^-$) was employed. Similar results are obtained in CH_3CN, when adding the same acid salts to **1** and monitoring by UV−vis spectroscopy (*vide infra*). The pK_a's of LuH^+-$CF_3SO_3^-$ and $Me_3NH^+Ph_4B^-$ in CH_3CN are 14.05 and 17.6, respectively;[36] thus the pK_a for deprotonation of the hydroxo bridge in **2** is roughly 14 < pK_a(**2**) < 17. In certain cases, it has been suggested that the aqueous pK_a would be 7.5 ± 1 pK_a units lower than in acetonitrile.[36] If this is approximately valid here and for CD_3CN, then the aqueous pK_a for **2** is crudely estimated as pK_a(**2**) ≅ 8 ± 2.5. By comparison to other oxo-bridged Mn, Fe, and Ru complexes, the μ-oxo group in **1** is quite basic: $[Mn^{IV}(\mu\text{-O})_n, (\mu\text{-OH})]_2^+$ (n = 1[36] or 2[37]) complexes have aqueous pK_a values (for deprotonation) ranging from about −2 to +7, while the values for $[Fe_2(OH)(O_2CCH_3)_2(HBpz_3)_2]^+$ [$HBpz_3$ = hydrotris(1-pyrazolyl)borate] and $[L'Ru(OH)(O_2CCH_3)_2FeL'']^{3+}$ (L′ = 1,4,7-triazacyclononane, L″ = 1,4,7-trimethyl-1,4,7-triazacyclononane) are estimated as pK_a ∼ 3.5.[38] A more accurate pK_a determination of **1**/**2** is limited by the availability of appropriate acids and the lability or inherent instability of the compounds (particularly **2**) and the solvents that need to be employed. However, such pK_a information may be of relevance to understanding proton transfer to and from heme-Cu oxidase turnover intermediates.[2] The potential key functional role of "drawing" protons by generation of an inherently strongly basic (O_2-derived) oxo group is obvious.

UV−Vis Spectroscopy. The interconversion of $[(F_8\text{-TPP})Fe^{III}-(O^{2-})-Cu^{II}(TMPA)]^+$ (**1**) and $[(F_8\text{-TPP})Fe^{III}-(OH^-)-Cu^{II}(TMPA)]^{2+}$ (**2**) by the addition of acid and base could also be monitored using UV−vis spectroscopy (Figure 3). Compound **1** exhibits a Soret band at 436 nm with an α-band at 554 nm. Addition of triflic acid converts this to μ-OH^- species **2**, possessing a Soret band at 408 nm with the α-band occurring at 570 nm (Figure 3b). This closely resembles the spectrum of the mononuclear $(F_8\text{-TPP})Fe^{III}-OH$ complex and is typical for high-spin $PFe^{III}-X$ complexes (X = monoanionic ligand). The addition of 1 equiv of triethylamine results in reconversion (>90%) to the μ-oxo-bridged complex **1** (Figure 3c). The red-shifted Soret band of **1** relative to **2** and other high-spin PFe^{III} complexes is attributed to the coordination of the dinegative oxo ligand and hence an increase of electron density at the metal center.[15c,39] The drastic change in the position of the Soret band upon addition of H^+ clearly implicates the oxo ligand as the site of the protonation, and not the nitrogen atoms of the pyridyl or porphyrinate ligands.

Extended X-ray Absorption Fine Structure (EXAFS) Spectroscopy. We previously[19] first noted the strong multiple scattering in both the Fe- and Cu-edge EXAFS Fourier transforms (i.e., unusually intense peaks at approximately R = 3.6 Å) corresponding to the Fe−Cu or Cu−Fe vector, respectively, ascribable to the linear Fe−O−Cu moiety in $[(F_8\text{-TPP})Fe^{III}-(O^{2-})-Cu^{II}(TMPA)]^+$ (**1**). A linear or slightly bent three-body system is particularly amenable to analysis of the observable multiple-scattering phenomenon, and such approaches have been utilized previously.[17a,25,40] Here, we present detailed EXAFS characterizations of **1** and **2** using *both* Cu- and Fe-edge EXAFS. Since $[(F_8\text{-TPP})Fe^{III}-(O^{2-})-Cu^{II}$-(TMPA)]$^+$ (**1**) can be generated by reaction of a preformed solution of a peroxo complex $[\{(TMPA)Cu^{II}\}_2(O_2)]^{2+}$ (**5**) and $(F_8\text{-TPP})Fe^{II}$,[21] and because **5** possesses oxygen atom ligands in a structurally characterized $TMPA-Cu^{II}$ environment (i.e., with pentacoordination, and a μ-1,2-peroxo ligand, Cu···Cu = 4.36 Å),[21] we compare the EXAFS spectroscopy of **5**, **1**, and **2**. For complexes **1** and **2**, Fe and Cu absorption edge data were collected to k = 16 $Å^{-1}$, resulting in good resolution of peaks in the Fourier transforms. Initial inspection of the raw data for

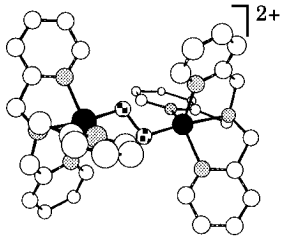

$[\{(L)Cu\}_2(O_2)]^{2+}$ **(5)**

(36) Baldwin, M. J.; Gelasco, A.; Pecoraro, V. L. *Photosynth. Res.* **1993**, *38*, 303−308 and references cited therein.

(37) Hage, R.; Krijnen, B.; Warnaar, J. B.; Hartl, F.; Stufkens, D. J.; Snoeck, T. L. *Inorg. Chem.* **1995**, *34*, 4973−4978.

(38) Turowski, P. N.; Armstrong, W. H.; Liu, S.; Brown, S. N.; Lippard, S. J. *Inorg. Chem.* **1994**, *33*, 636−645 and references cited therein.

(39) Burstyn, J. N.; Roe, J. A.; Miksztal, A. R.; Shaevitz, B. A.; Lang, G.; Valentine, J. S. *J. Am. Chem. Soc.* **1988**, *110*, 1382−1388.

(40) (a) Han, J.; Blackburn, N. J.; Loehr, T. M. *Inorg. Chem.* **1992**, *31*, 3223−3229. (b) Alexiev, V. D.; Binsted, N.; Cook, S. L.; Evans, J.; Price, R. J.; Clayden, N. J.; Dobson, C. M.; Smith, D. J.; Greaves, G. N. *J. Chem. Soc., Dalton Trans.* **1988**, 2649−2654. (c) Cook, S. L.; Evans, J.; McNulty, G. S.; Greaves, G. N. *J. Chem. Soc., Dalton Trans.* **1986**, 7−14. (d) Pettingill, T. M.; Strange, R. W.; Blackburn, N. J. *J. Biol. Chem.* **1991**, *266*, 16996−17003. (e) Westre, T. E.; Di Cicco, A.; Filliponi, A.; Natoli, C. R.; Hedman, B.; Solomon, E. I.; Hodgson, K. O. *J. Am. Chem. Soc.* **1994**, *116*, 6757−6768.

Table 1. Comparison of EXAFS and X-ray Structure Distances (Å) and Angles (deg) for $[\{(TMPA)Cu\}_2(O_2)]^{2+}$ (**5**), $[(F_8\text{-}TPP)Fe^{III}-(O^{2-})-Cu^{II}(TMPA)]^{+}$ (**1**), and $[(F_8\text{-}TPP)Fe^{III}-(OH^{-})-Cu^{II}(TMPA)]^{2+}$ (**2**)

$[\{(TMPA)Cu\}_2(O_2)]^{2+}$ (**5**)		
	EXAFS	X-ray
4N	2.05 ± 0.02	2.078(7) (av)
1O	1.85 ± 0.02	1.852(5)

$[(F_8\text{-}TPP)Fe^{III}-(O^{2-})-Cu^{II}(TMPA)]^{+}$ (**1**)			$[(F_8\text{-}TPP)Fe^{III}-(OH^{-})-Cu^{II}(TMPA)]^{2+}$ (**2**)	
	EXAFS (Cu edge)	X-ray		EXAFS (Cu Edge)
4N	2.06 ± 0.02	2.066(7) (av)	4N	2.02 ± 0.02
1O	1.83 ± 0.02	1.856(5)	1O	1.89 ± 0.02
1Fe	3.56 ± 0.03	3.596(2)	1Fe	not seen
∠Cu−O−Fe	176 ± 5	178.2(4)		

$[(F_8\text{-}TPP)Fe^{III}-(O^{2-})-Cu^{II}(TMPA)]^{+}$ (**1**)			$[(F_8\text{-}TPP)Fe^{III}-(OH^{-})-Cu^{II}(TMPA)]^{2+}$ (**2**)	
	EXAFS (Fe edge)	X-ray		EXAFS (Fe edge)
4N	2.09 ± 0.02	2.106(7) (av)	4N	2.05 ± 0.02
1O	1.72 ± 0.02	1.740(5)	1O	1.87 ± 0.02
1Cu	3.54 ± 0.05	3.596(2)	1Cu	3.66 ± 0.03
∠Fe−O−Cu	172 ± 10	178.2(4)	∠Fe−O−Cu	157 ± 5 154 (triangulation; see text)

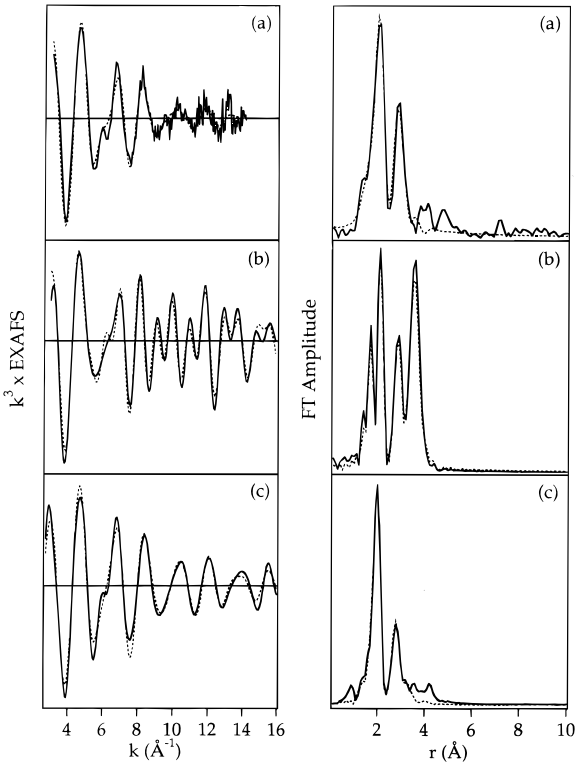

Figure 4. Experimental (solid) versus simulated (dashed) Cu K-EXAFS and Fourier transforms for (a) $[\{(TMPA)Cu\}_2(O_2)]^{2+}$ (**5**), (b) $[(F_8\text{-}TPP)Fe^{III}-(O^{2-})-Cu^{II}(TMPA)]^{+}$ (**1**), and (c) $[(F_8\text{-}TPP)Fe^{III}-(OH^{-})-Cu^{II}(TMPA)]^{2+}$ (**2**).

1 and **2** indicated significant unresolved intensity in the transforms above 4 Å (no phase shift applied) arising from scattering off atoms at distances greater than 4.5−5 Å from Cu or Fe. It is likely that this intensity arises from porphyrin atoms at the Cu edge or TMPA atoms at the Fe edge, which would be almost impossible to simulate. For this reason, raw data for **1** and **2** were Fourier filtered from 0 to 4.0 Å (phase uncorrected) at both Cu and Fe edges, and all simulations were carried out on these Fourier-filtered data sets.

EXAFS of $[\{(TMPA)Cu^{II}\}_2(O_2)]^{2+}$ (5) and $[(F_8\text{-}TPP)Fe^{III}-(O^{2-})-Cu^{II}(TMPA)]^{+}$ (1). Parts a and b of Figure 4 show the Cu K-EXAFS and Fourier transforms of **5** and **1**, respectively. Close inspection of these shows that the major difference arises from the presence in **1** of (i) a splitting of the first peak in the FT and (ii) an intense outer-shell contribution at ca. 3.5 Å, which translates into a high-frequency oscillation in the EXAFS. This oscillation becomes more intense at high *k* and, consequently, is probably due to a Cu−Fe interaction.

A simulation of the EXAFS of $[\{(TMPA)Cu^{II}\}_2(O_2)]^{2+}$ (**5**) is also given in Figure 4a. This requires four low-*Z* atoms (nitrogens) at 2.05 Å, one low-*Z* atom (oxygen) at the shorter distance of 1.85 Å (Table 1), and outer-shell contributions from two pyridyl ligands at the expected distances.[41] Only single-scattering contributions appeared necessary to simulate these outer-shell C atoms. We have consistently noted that whereas Cu(I) complexes of imidazolyl, pyridyl, and pyrazolylborate type ligands exhibit strong outer-shell contributions which can only be simulated by including the multiple-scattering interactions, the copper(II) complexes of these ligands usually exhibit dramatically attenuated MS contributions.[42] We have interpreted this attenuation as the result of dynamic disorder arising from Jahn−Teller effects; thus, axial−equatorial interconversions in the copper(II) complexes will result in a large spread in outer-shell distances and a consequent large increase in Debye−Waller terms terms for the outer-shell contributions.

The results of the simulation of $[\{(TMPA)Cu^{II}\}_2(O_2)]^{2+}$ (**5**) were used as the starting point for the simulation of the Cu K-EXAFS of $[(F_8\text{-}TPP)Fe^{III}-(O^{2-})-Cu^{II}(TMPA)]^{+}$ (**1**). The first-shell analysis placed four low-*Z* (N) atoms at 2.06 Å, essentially the same distance as in the starting complex **5**, and the short O atom refined to 1.83 Å, somewhat less than the $Cu-O_{peroxo}$ distance of 1.85 Å observed for **5**, *vide supra*. These EXAFS-derived bond distances in **1** are also summarized in Table 1, where data derived from the X-ray crystallographic study on **1**[15c] are compared. Initial attempts to simulate the

(41) In addition to the first-shell contributions, the simulation required four C atoms at 2.84 Å. In addition, two C atoms at 3.30 Å were necessary to reproduce the second shell in the transform, probably derived from the connecting methylene C atoms between the pyridyl groups of the ligand. An equivalent simulation could be achieved by including all the single and MS contributions from three pyridyl groups with Cu−N(py) = 2.06 ± 0.02 Å, but because of the rather large spread in Cu−N distances found in the crystal structure of $[\{(TMPA)Cu^{II}\}_2(O_2)]^{2+}$ (**5**) [2.024(7)−2.102(6) Å], we believe that the detailed MS analysis, with its large increase in the number of adjustable parameters, is not justified in the present case. Complete details of the parameters used in the simulation can be found in Table S2 of the supporting information.

(42) Blackburn, N. J.; Strange, R. W.; Farooq, A.; Haka, M. S.; Karlin, K. D. *J. Am. Chem. Soc.* **1988**, *110*, 4263−4272.

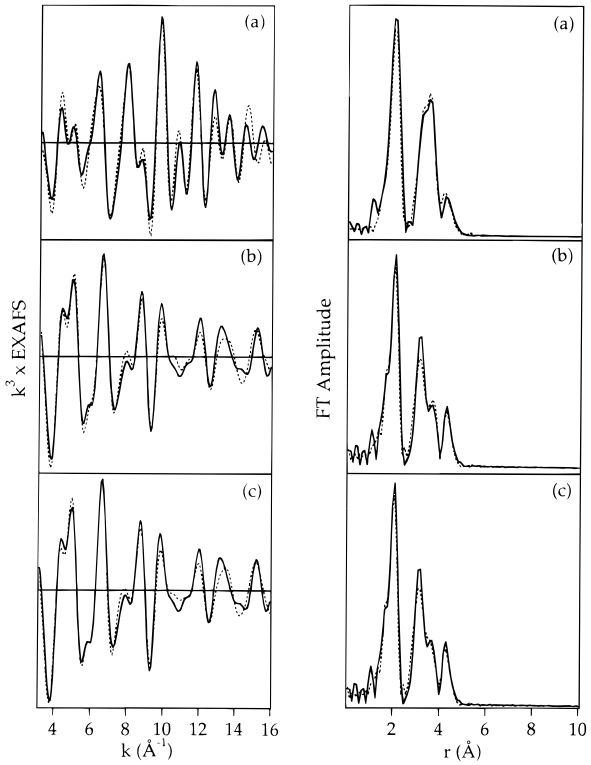

Figure 5. Experimental (solid) versus simulated (dashed) Fe K-EXAFS and Fourier transforms for (a) [(F_8-TPP)Fe^{III}−(O^{2-})−Cu^{II}(TMPA)]$^+$ (**1**); (b) [(F_8-TPP)Fe^{III}−(OH^-)−Cu^{II}(TMPA)]$^{2+}$ (**2**), simulated with no Fe−OH−Cu multiple-scattering interaction and Fe−Cu = 3.72 Å; and (c) [(F_8-TPP)Fe^{III}−(OH^-)−Cu^{II}(TMPA)]$^{2+}$ (**2**), simulated with a contribution from a Fe−OH−Cu multiple-scattering pathway, Fe−Cu = 3.66 Å, ∠Fe−OH−Cu = 157°.

intense outer-shell contribution by a single-scattering contribution from a Cu−Fe interaction required a Debye−Waller term close to 0, with Cu···Fe = 3.60 Å. Since the Fe−O distance derived from analysis of the Fe K-edge spectrum was 1.72 Å (*vide infra*), this Cu···Fe distance would require a linear Cu−O−Fe interaction and, consequently, a strong MS contribution from the collinear triatom grouping. Thus, we continued the refinement of the simulation by including a Cu−O−Fe multiple-scattering interaction, with the metal−metal distance and ∠Cu−O−Fe angle as adjustable parameters. Least-squares refinement resulted in the simulation shown in Figure 4b and Cu···Fe = 3.56 ± 0.03 Å and ∠Cu−O−Fe = 176 ± 5° (Table 1). This gives an excellent fit to the Fourier transform, and to the EXAFS except around k = 6−7.5 Å^{-1}; we believe that the small discrepancies between experimental and simulated spectra in this region are due to small inaccuracies in the k-dependence of the phases or atomic potentials for the Cu−Fe interaction.

Simulation of the Fe K-EXAFS of [(F_8-TPP)Fe^{III}−(O^{2-})−Cu^{II}(TMPA)]$^+$ (**1**) is shown in Figure 5a. Here, the pyrrole C_γ outer-shell atoms are expected to contribute to both single and multiple scattering (∠Fe−N_α−C_γ = 158°), while the meso C atoms which carry the aryl substituents will contribute to the single scattering, and our simulation includes these contributions at the expected distances. The Fe first-shell coordination includes four N (pyrrole) atoms at 2.09 Å and the very short oxygen atom with Fe−O = 1.72 Å. As for the Cu edge, satisfactory simulation of the outer shells requires a multiple-scattering contribution from Fe−O−Cu. Least-squares refinement leads to Fe···Cu = 3.54 ± 0.05 Å and ∠Fe−O−Cu = 172 ± 10° (Table 1). The Fe-edge simulation is less precise than the Cu-edge simulation, since the Fe···O−Cu and Fe−C shells interfere and are highly correlated. Nevertheless, the intermetal metrical details are remarkably consistent with the results from the Cu edge.

The very short Fe−O bond length (1.72 Å, Table 1) derived from the Fe K-EXAFS and X-ray diffraction study[15c] is typical of oxo-bridged iron homo- or hetero-dinuclear complexes.[35,43] As discussed, the results of the MS analysis strongly support an almost linear Fe−O−Cu bridge with an angle close to 172°. However, if we consider the Cu−O bond distance (Cu edge), the Fe−O bond length (Fe edge), and the Cu···Fe distance (Cu edge) as "hard" data, this leads (by triangulation) to an estimate of the ∠Fe−O−Cu angle of 178°, in fact, the value found by X-ray crystallography (Table 1).

EXAFS of [(F_8-TPP)Fe^{III}−(OH^-)−Cu^{II}(TMPA)]$^{2+}$ (2). The strong multiple-scattering contribution observed for the EXAFS of [(F_8-TPP)Fe^{III}−(O^{2-})−Cu^{II}(TMPA)]$^+$ (**1**), which was due to the virtually linear Fe−O−Cu moiety, is notably absent (Fourier transform, Figure 4c) in the Cu K-EXAFS of **2**; this strongly implies that the Fe−(OH)−Cu moiety in this compound is *not* similarly linear. Detailed simulations at both the Cu and Fe edges of **2** have been carried out to probe the differences in structure. At the Cu edge, a good simulation of the data cannot be achieved with either Cu−O−Fe multiple scattering or Cu−Fe single scattering; i.e., the metal−metal interaction is unobservable by EXAFS. The results are shown in Figure 4c and Table 1, where strong similarities to the EXAFS of [{(TMPA)-Cu^{II}}$_2$(O_2)]$^{2+}$ (**5**) are apparent. The most notable change in the copper coordination sphere of **2**, relative to **1** or **5**, is a lengthening of the Cu−O bond distance to 1.89 Å. These observations are consistent with protonation of the Cu−O−Fe bridge, leading to significant bending such that a dramatic attenuation of the MS occurs. No estimate of the ∠Cu−(OH)−Fe angle could be obtained from the Cu-edge data, since the Cu−Fe interaction was not observable.

Simulations at the Fe edge were more successful in establishing the metal−metal distance and the ∠Fe−(OH)−Cu angle in [(F_8-TPP)Fe^{III}−(OH^-)−Cu^{II}(TMPA)]$^{2+}$ (**2**). Figure 5b,c shows Fe-edge EXAFS and Fourier transforms of **2**. Initial simulations presumed that, as for the Cu-edge data, no multiple-scattering contribution would be present. However, in this case, satisfactory simulation (Figure 5b) absolutely required the inclusion of a Fe−Cu single-scattering contribution at 3.72 ± 0.05 Å, with an Fe−O bond of 1.87 Å, significantly longer than the value (1.72 Å) determined for the μ-oxo [(F_8-TPP)Fe^{III}−(O^{2-})−Cu^{II}(TMPA)]$^+$ (**1**). Triangulation using the EXAFS-determined values for Cu−O (1.89 Å), Fe−O (1.87 Å), and Fe···Cu (3.72 Å) gives a calculated ∠Fe−O−Cu angle of 163°. Since we would expect a moderate MS contribution from a triatom group at this angle, we resimulated the EXAFS of **2** including an Fe−O(H)−Cu interaction with the Fe···Cu distance and ∠Fe−O−Cu angle as adjustable parameters. The best fit was obtained with Fe···Cu = 3.66 ± 0.03 Å and ∠Fe−O(H)−Cu = 157 ± 5°. From triangulation using these three distances, we calculate an angle of 154°, in excellent agreement with the simulation (Figure 5c).

Absorption Edges of [(F_8-TPP)Fe^{III}−(O^{2-})−Cu^{II}(TMPA)]$^+$ (1) and [(F_8-TPP)Fe^{III}−(OH^-)−Cu^{II}(TMPA)]$^{2+}$ (2). Figure S1 (supporting information) compares the Cu K edges of **1** and **2**. Both edges are typical of Cu(II) complexes with a weak 1s → 3d pre-edge feature and an almost featureless absorption edge, centered on ~8990 eV. Significantly, the two edges are almost superimposable below 9000 eV, suggesting strong similarities in geometric structure. This is consistent with the EXAFS simulations, in which a small (0.04 Å) variation in Cu−O distance is the only real difference (apart from the ∠Cu−O−

(43) West, B. O. *Polyhedron* **1989**, *8*, 219−274.

Fe angle). The Fe edges are compared in Figure S2 (supporting information), and these also show strong similarities in the main absorption between 7120 and 7140 eV. In the Fe case, however, differences are apparent in the pre-edge feature centered at 7113 eV. The pre-edge of the linear-bridged oxo compound is about twice as intense as for the bent hydroxo-bridged compound. Previously observed differences in pre-edge intensity of iron(III) complexes have been correlated with coordination number and site symmetry.[44] Thus, for example, Westre and coworkers[44b] report a similar difference in intensity between Fe(III)−bleomycin or the high-spin iron(III) complex Na[Fe(H_2O)(EDTA)] and the distorted octahedral complex Fe(L″)(NO)$(N_3)_2$, which has a similarly short Fe−X (X = NO) distance of 1.74 Å. The difference in intensity is interpreted as arising from compression of the axial ligation, resulting in significant lowering of the formally octahedral symmetry. The results of the present study emphasize that, in porphyrin systems at least, the origin of the increase in intensity of the 1s → 3d feature must be due to the short axial bond itself, rather than a decrease in symmetry from O_h to C_{4v} (as the result of a decrease in coordination number from 6 to 5), because the iron in both complexes **1** and **2** is five coordinate (C_{4v}), and changes in axial bond length thus have no effect on the formal symmetry of the complex.

Structure of the Hydroxo Complex [(F_8-TPP)Fe^{III}−(OH^-)−Cu^{II}(TMPA)]$^{2+}$ (2) and Comparisons to Related Systems. A comparison of the EXAFS-derived structural parameters of bent μ-OH^- **2** with X-ray structure derived parameters for [(F_8-TPP)Fe^{III}−(O^{2-})−Cu^{II}(TMPA)]$^+$ (**1**) merits further discussion (Table 1). Thus, on going from Fe−O−Cu to Fe−(OH)−Cu (in **1** vs **2**), the Fe−O bond distance lengthens considerably, from 1.74 to 1.87 Å. The corresponding Cu−O distance increases by only ∼0.03 Å, from 1.86 to 1.89 Å. These increases are attributed to a diminution of anionic charge (from 2− to 1−) on the μ-oxo ligand upon protonation. In the case of Fe−O, however, an added dominant contributing feature to bond lengthening is the implicit loss of some π-bonding from O to Fe in accord with the requirements of rehybridization about O [from the implicit "sp" of linear Fe−O−Cu toward sp^2 in bent Fe−(OH)−Cu]. Since the oxo group cannot "π-bond" to Cu^{2+} (d^9) in complex **1** because all orbitals of π-symmetry on the metal are already filled, we observe only the small "electrostatic" change (∼0.03 Å) in Cu−O that attends protonation. It is likely that this effect also contributes to the decrease in pre-edge intensity upon protonation, since there is less mixing of oxo p(π) character into the d-shell, such that the transition becomes more strongly forbidden. Such effects have been well documented in (TPP)V═O and (TPP)Cr═O species, where an intense pre-edge feature results from the strong oxygen p(π) mixing into the d-shell, although corresponding data for similar ferryl (Fe═O) derivatives are conflicting.[45] The average Cu−N_{ligand} distances for **2** (2.02 Å) are consistent with those expected for Cu^{II}−N. The diminished "pull" of the μ-OH^- ligand is apparent also in the smaller Fe−N distances (2.05 Å in **2** vs 2.09 Å in **1**), but we are unable to measure an expected decrease in the Fe−N_4 (mean porphyrin plane) distance for **2**.

While other Fe−OH−Cu species have been proposed,[16a,g,46] [(OEP)Fe^{III}−(OH^-)−Cu^{II}(Me_5dien)($OClO_3$)]$^+$ has been characterized by X-ray crystallography and EXAFS spectroscopy.[17a] Its structural parameters can be compared to those of a μ-oxo species [(OEP)Fe^{III}−(O^{2-})−Cu^{II}(Me_6tren)]$^+$,[17] as well as to **1** and **2**. The Fe···Cu distance in [(OEP)Fe^{III}−(OH^-)−Cu^{II}(Me_5dien)($OClO_3$)]$^+$ is somewhat longer that that for **2** [3.804 Å (crystal) vs 3.66 Å (EXAFS), respectively]. Since the ∠Fe−(OH)−Cu angles are quite similar [157° for [(OEP)Fe^{III}−(OH^-)−Cu^{II}(Me_5dien)($OClO_3$)]$^+$],[17a] elongation of the Fe···Cu distance is due to the longer metal−O(H) bond lengths; Fe−O(H) = 1.93 Å and Cu−O(H) = 1.95 Å in [(OEP)Fe^{III}−(OH^-)−Cu^{II}(Me_5dien)($OClO_3$)]$^+$, and corresponding values in **2** are 1.87 and 1.89 Å (Table 1). Differences in the porphyrinates or copper ligands employed are presumed to be responsible. Note, however, that the Fe···Cu distance in [(OEP)Fe^{III}−(O^{2-})−Cu^{II}(Me_6tren)]$^+$ (3.57 Å) is essentially the same as found for [(F_8-TPP)Fe^{III}−(O^{2-})−Cu^{II}(TMPA)]$^+$ (**1**) (3.60 Å).

A further interesting comparison between the two sets of F_8-TPP and OEP complexes is the Cu−O bond length changes. This value only increases by 0.03 Å on going from [(F_8-TPP)Fe^{III}−(O^{2-})−Cu^{II}(TMPA)]$^+$ (**1**) to [(F_8-TPP)Fe^{III}−(OH^-)−Cu^{II}(TMPA)]$^{2+}$ (**2**). The corresponding increase on going from [(OEP)Fe^{III}−(O^{2-})−Cu^{II}(Me_6tren)]$^+$ to [(OEP)Fe^{III}−(OH^-)−Cu^{II}(Me_5dien)($OClO_3$)]$^+$ is 0.12 Å. The Fe−O distances also change by a greater extent (0.19 vs 0.13 Å). These facts might explain the fully reversible acid−base interconversion chemistry exhibited by the **1** and **2** pair, a phenomenon not observed in the OEP complexes. We note that the μ-oxo and μ-hydroxo OEP compounds possess different ligand donors on their respective copper(II) atoms, and strictly analogous sets of compounds have not yet (to our knowledge) been compared.

The XAS study of [(OEP)Fe^{III}−(O^{2-})−Cu^{II}(Me_6tren)]$^+$ and [(OEP)Fe^{III}−(OH^-)−Cu^{II}(Me_5dien)($OClO_3$)]$^+$ utilizes a newly described multiple-scattering methodology, GNXAS, to calculate contributions to the Fe-edge EXAFS of these compounds.[17a] Comparable agreement with the crystallographic distances and bridge angle for the oxo-bridged complex was obtained relative to the present study, but less conclusive results were obtained on the bent hydroxo-bridged species. One reason for this may be the longer Fe···Cu distance in [(OEP)Fe^{III}−(OH^-)−Cu^{II}(Me_5dien)($OClO_3$)]$^+$ relative to that observed in [(F_8-TPP)Fe^{III}−(OH^-)−Cu^{II}(TMPA)]$^{2+}$ (**2**) (*vide supra*). By including data at the Cu edge, we have been able to introduce additional parameters, the Cu−O and Cu···Fe distances, and the ∠Cu−O−Fe angle in [(F_8-TPP)Fe^{III}−(O^{2-})−Cu^{II}(TMPA)]$^+$ (**1**), which have provided valuable cross checks on the validity of our calculations and enabled us to provide a clear structural representation of **2** (*vide supra*) in the absence of an X-ray crystal structure. The MS methodology used in the present study is the same as that applied by us and others for the exact simulation of raw EXAFS data of metal−histidyl and metal−pyridyl,[25,42,47] metal−carbonyl,[40b−d] and metal−cyano[40a] derivatives in proteins and model complexes for over a decade. The present work provides further validation of these earlier results.

Comparisons with XAS Data on a Heme-Copper Oxidase. Recently, we have carried out a detailed EXAFS and ENDOR investigation of the Cu_B site in quinol oxidase aa_3-600 from *B. subtilis*.[5d] In this isolated heme-Cu oxidase, the magnetic coupling between Fe and Cu is broken at high pH (8.8), leading to observable EPR signals from both Fe_{a3} and Cu_B. The EXAFS data is insensitive to variation in pH from 7 to 8.8, suggesting that the ligation around Cu_B is the same in the coupled (as isolated enzyme) and the higher pH uncoupled form of the

(44) (a) Roe, A. L.; Schneider, D. J.; Mayer, R. J.; Pyrz, J. W.; Widom, J.; Que, L. J., Jr. *J. Am. Chem. Soc.* **1984**, *106*, 1676−1681. (b) Westre, T. E.; Loeb, K. E.; Zaleski, J. M.; Hedman, B.; Hodgson, K. O.; Solomon, E. I. *J. Am. Chem. Soc.* **1995**, *117*, 1309−1313.

(45) Penner-Hahn, J. E.; Hodgson, K. O. In *Physical Inorganic Chemistry Series, Iron Porphyrins*; Lever, A. P. B., Gray, H. B., Eds.; VCH: New York, 1989; Part III; pp 235−304.

(46) Lukas, B.; Miller, J. R.; Silver, J.; Wilson, M. T.; Morrison, I. E. G. *J. Chem. Soc., Dalton Trans.* **1982**, 1035.

(47) (a) Blackburn, N. J.; Strange, R. W.; McFadden, L. M.; Hasnain, S. S. *J. Am. Chem. Soc.* **1987**, *109*, 7162−7170. (b) Reedy, B. J.; Blackburn, N. J. *J. Am. Chem. Soc.* **1994**, *116*, 1924−1931.

dinuclear center. The results support a Cu_B coordination of three histidines and one O-donor ligand carrying an exchangeable proton(s) such as water or hydroxide (OH^-). The best fit for the three N(imidazole)/one O(hydroxyl) structure required a Cu−O(hydroxyl) bond length of 1.92 ± 0.03 Å, closely resembling the Cu−O bond length (1.89 ± 0.02 Å) determined for $[(F_8\text{-TPP})Fe^{III}-(OH^-)-Cu^{II}(TMPA)]^{2+}$ (**2**), but much longer than the Cu−O bond length (R_{cryst} = 1.856(5) Å) in $[(F_8\text{-TPP})Fe^{III}-(O^{2-})-Cu^{II}(TMPA)]^{+}$ (**1**). In addition, *no* intense outer-shell scattering is observed in the Fourier transform of the aa_3-600 Cu_B EXAFS. We conclude that whereas the enzyme cannot contain a linear oxo bridge, bent oxo or hydroxo is fully consistent with the available data for the enzyme; we cannot, however, entirely rule out the possibility of having a large (>∼3.5 Å) Fe···Cu separation. The Fe absorption edge for cytochrome aa_3-600 (Figure S2 and inset, supporting information) also supports the μ-OH^- model, since the intensity of the pre-edge feature is close to that of **2**.[48] Thus, in these initiatory but first direct comparisons of the EXAFS of model compounds with enzyme preparations, further support for the $Fe^{III}-(OH^-)-Cu^{II}$ moiety as an "as-isolated" structure form of heme-Cu oxidases is provided.

Additional XAS Comment. It is curious that the magnitude of the Fe−(OH)−Cu three-body MS interaction is so different in the Fe and Cu EXAFS of $[(F_8\text{-TPP})Fe^{III}-(OH^-)-Cu^{II}(TMPA)]^{2+}$ (**2**). One possible explanation lies in the fact that the porphyrinate ligand may provide a much more rigid environment for Fe than does the TMPA ligand for Cu. Thus, molecular vibrations of the Fe coordination sphere may be more highly correlated, leading to smaller Debye−Waller factors at Fe than at Cu. However, at this time we do not fully understand the origins for the observed differences in multiple-scattering intensities in the Fe and Cu EXAFS. Paradoxically, this may imply that while interpretation of the Fe EXAFS of the enzymes is complicated by the contribution from the Fe_a heme component, determination of bridging geometry from any putative bridging ligand may only be possible using Fe-edge EXAFS data. Further work is underway to understand the factors influencing the magnitude of MS interactions in heterobimetallic complexes.

Summary/Conclusion

The cytochrome *c* oxidase enzyme X-ray crystal structures[7−9] do not reconcile previous interpretations of EPR/magnetic data on "isolated" protein preparations,[13] underscoring the need for biomimetic and spectroscopic approaches such as detailed in this paper. Thus, heterobimetallic μ-O^{2-}- and μ-OH^--bridged complexes described here are good models for probing heme-Cu structures and chemistry relevant to the enzymes. We can summarize the main conclusions and advancements:

We have established the *reversible* acid−base interconversion of $[(F_8\text{-TPP})Fe^{III}-(O^{2-})-Cu^{II}(TMPA)]^{+}$ (**1**) and $[(F_8\text{-TPP})Fe^{III}-(OH^-)-Cu^{II}(TMPA)]^{2+}$ (**2**), by rigorous synthetic chemistry, and through ^{1}H-NMR and UV−vis titrations. Such behavior is not seen for related systems.[17a]

Established XAS MS analytical techniques, using both Fe and Cu edges, provide a powerful and accurate approach to the determination of the identity and coordination geometry of potential bridging ligands. These reveal elongated metal−O(H) bond distances in **2** relative to **1**, the expected bending from near-linearity to give ∠Fe−O(H)−Cu = 157 ± 5°, and the consequent increase in Fe···Cu from 3.596(2) Å (X-ray) to 3.66 ± 0.03 Å in **2**. Notably, the very intense Fourier transform peak due to Fe−Cu and Cu−Fe MS interactions (i.e., focusing effect) at R = ∼3.6 Å seen in **1** is absent in **2**, because of this bending.

The relationship and difference in physical properties (UV−vis, ^{1}H NMR, and magnetism) of **1** and **2** has been ascertained. An NMR titration of **1** with H^+ points to protonation being slow on the NMR time scale. The oxo group in **1** is more basic than in other oxo-bridged metallic systems; the aqueous pK_a for deprotonation of **2** is estimated as 8 ± 2.5. Such information and protonation (deprotonation) chemistry of bridging (or coordinated) ligands could well be important in heme-Cu oxidase function.[2a,7]

The XAS properties of $[(F_8\text{-TPP})Fe^{III}-(OH^-)-Cu^{II}(TMPA)]^{2+}$ (**2**), in particular, compare well with those observed for an enzyme preparation from the quinol oxidase aa_3-600 from *B. subtilis*. Thus, structural and magnetic characteristics make such μ-OH^- species strong candidates for resting state enzyme mimics. Additional demonstration of reversible protonation events between **1** and **2** provides a basis for proposal of these complexes as models for turnover intermediates,[2a] which might precede or coincide with the "resting state". Ongoing studies concern the generation, characterization, reactivity studies, and enzyme comparisons with additional porphyrinate−Fe/Cu dinuclear species.

Acknowledgment. This research has been supported by National Institutes of Health Grants NS27583 (N.J.B.) and GM28962 (K.D.K.); M.W. acknowledges the Sigrid Juselius Foundation and the Academy of Finland (MRC).

Supporting Information Available: Tables S1−S7 with parameters used in the data collection and simulation of the EXAFS and Fourier transforms at either the Fe or Cu K-edge of compounds **1**, **2**, and **5** and Figures S1 and S2 with Cu and Fe K-absorption edges for **1**, **2**, and the protein preparation (10 pages). This material is contained in many libraries on microfiche, immediately follows this article in the microfilm version of the journal, can be ordered from the ACS, and can be downloaded from the Internet; see any current masthead page for ordering information and Internet access instructions.

JA951686B

(48) However, these latter data represent the average of the pre-edge of the six-coordinate heme *a* and heme a_3 and are thus not directly comparable with **2**.